PCCP

Accepted Manuscript

ROYAL SOCIETY
OF CHEMISTRY

www.rsc.org/pccp

Journal Name

Physical Chemistry Chemical Physics

Dynamic Article Links▶

ARTICLE TYPE

Facile synthesis of highly conductive sulfur-doped reduced graphene oxide sheets

Zhengshan Tian,[ab] Jitao Li,[b] Gangyi Zhu,[b] Junfeng Lu,[b] Yueyue Wang,[b] Zengliang Shi[b] and Chunxiang

5 **Xu*[b]**

A facile hydrothermal strategy to synthesize sulfur-doped reduced graphene oxide (S-RGO) sheets with good conductivity is proposed by only using graphene oxide (GO) sheets and sodium sulphide (Na_2S) as
10 precursors through a hydrothermal reaction process at 200 °C in one pot. The introduced Na_2S can act as not only a sulfur dopant, but also a high-efficient reducing agent in the formation of S-RGO sheets, which improves dramatically the electrical conductivities of the resulting S-RGO sheets, compared with other previous reports. The current arrives about 50.0 mA at an applied bias of 2.0 V for the optimized sample with 2.22 at% sulfur doping. This current value is much higher than that of RGO sheets (~ 1.2 mA)
15 annealed at 200 °C and very close to that of the single-layer graphene sheet (~ 68.0 mA) grown by chemical vapor deposition under the same test conditions. The resulting highly conductive S-RGO sheets offer many promising technological applications such as efficient metal-free electrocatalysts in oxygen reduction reaction for fuel cells and supercapacitor electrode materials for high-performance Li-ion batteries.

Introduction

20 Graphene, a monolayer of carbon atoms arranged in a honeycomb lattice, has attracted considerable interest owing to its excellent chemical, mechanical and thermal properties and potential applications in a wide range of fields, such as electronics,[1,2]
25 sensors,[3] batteries,[4,5] and catalysts.[6,7] However, the zero band gap of graphene weakens its applications.[8] Fortunately, numerous efforts have been made to modify its electrical property and chemical activity. The chemical doping of graphene or GO sheet with heteroatoms is considered as an effective strategy to tailor its
30 electronic environment and its intrinsic properties.[9,10] It is found that the difference in electronegativity between carbon atoms and heteroatoms (S, N, B, P, Cl, Br, I) can polarize adjacent carbon atoms to obtain a wider band gap.[7,11,12]

On the other hand, as a two-dimensional monolayer form of
35 sp^2 and sp^3 hybridized carbon atoms linked covalently with oxygen-containing groups,[13] GO sheet has now become a more promising basic building block to fabricate multi-functional graphene-based derivates because of its low cost, easy preparation, scalable production, high processability, and
40 dispersibility in water and polar organic solvents;[14] moreover, it is traditionally served as a precursor for graphene. Reduced graphene oxide (RGO) sheet exhibits both advanced chemical and physical adsorption capability due to the abundant functional groups and high electrical conductivity of its well-developed sp^2
45 networks.[15] Thus, increasing focus is being given to the provision of graphene by the reduction of GO sheet as a facile method for possible large scale production.

More recently, lots of S-doped graphene-based materials have gained the considerable interest because of a wider band gap
50 derived from the electron-withdrawing character of S.[16] These S-doped carbon materials can exhibit superior catalytic activity as metal-free electrocatalysts in oxygen reduction reaction (ORR) for fuel cells[17-22] and higher Li storage capacity as anode materials in Li ion batteries.[23-25] For example, Yang et al.[7]
55 synthesized the sulfur-doped graphene with excellent catalytic activity in alkaline media for ORRs by directly annealing GO sheet and benzyl disulfide at 600-1050 °C in argon. Pumera and his colleagues[16] prepared the sulfur-doped graphene with electrocatalysis for ORRs via thermal exfoliation of graphite
60 oxide in SO_2, H_2S or CS_2 gas atmosphere at high temperature. Moreover, Wang and his co-workers[21] obtained S-doped graphene from a cycled lithium-sulfur battery in which graphene-sulfur composites were used as cathode materials. However, most sulfur dopants such as benzyl disulfide,[7,26] SO_2, H_2S,[27] CS_2[16] and
65 thiophene[28] utilized in various synthesis methods often involve chemical vapor deposition (CVD) and/or thermal annealing

performed at high temperature under gas phases, which require rigorous conditions or special instruments, and the scale-up production is limited. Therefore, using effective sulfur source to prepare sulfur-doped graphene on a large scale through a facile
5 hydrothermal process is still highly desired.

In the present study, we demonstrated the successful fabrication of S-RGO sheets by directly using GO sheets and Na_2S as precursors through a facile hydrothermal reaction in one pot. During the hydrothermal reaction process, the introduced
10 Na_2S acted as not only a sulfur dopant, but also a reducing agent in the formation of S-RGO sheets. The synergistic effects of a sulfur dopant and a reducing agent enhanced dramatically the electrical conductivities of the resulting S-RGO sheets.

Experimental Section

15 **Preparation of the samples**

The S-RGO sheets were synthesized by only using GO sheets and Na_2S as precursors through a hydrothermal reaction at 200 °C in one pot. Firstly, without any polymer or surfactant, a homogeneous GO aqueous solution (3 mg mL^{-1}) was obtained by
20 controlling ultrasonication-assisted exfoliation of graphite oxides in deionized water, which were synthesized from graphite powders based on a modified Hummers' method.[29] Then, a given amount of Na_2S was introduced into 80 mL GO aqueous solution under magnetic stirring at 25 °C for 10 min, subsequently the
25 above mixture solution was transferred and sealed into a Teflon-lined stainless steel autoclave (100 mL), heating to 200 °C and maintaining at this temperature for 10 h to obtain a dispersion containing S-RGO sheets. Thirdly, the resulting dispersion containing S-RGO sheets was naturally cooled to room
30 temperature, purified by filtration and washed with deionized water several times. Finally, the resulting S-RGO sheets were obtained after air drying. The atomic percentage of S in the resulted S-RGO sheets was readily controlled by adjusting the initial amount of Na_2S in the parent mixture solution. The
35 resulted ratio of S was changed gently from 0 to 2.22 at% as 0-27 mg Na_2S was added gradually to 80 mL GO aqueous solution (3 mg mL^{-1}). As the amount of the initial Na_2S was excessive over 27 mg, the S content in the S-RGO sheets would be saturated at the maximum of 2.22 at%. For comparison, RGO sheets were
40 also synthesized under the same condition as that of S-RGO sheets without adding Na_2S. A single-layer graphene sheet was synthesized by a CVD method.[30]

Characterization

45 The morphologies and structures of the samples were characterized by a scanning electron microscope (SEM, Hitachi S-4800) equipped with energy dispersive X-ray spectroscopy (EDX), a transmission electron microscope (TEM, JEM-2100), and a X-ray diffractometer (XRD, Bruker D8 Discover) with Cu
50 Ka radiation (1.5406 Å). X-ray photoelectron spectroscopy (XPS,

ESCALAB 250Xi), Raman spectrum with an excitation laser of 514.5 nm (LabRAM HR800) and Fourier transform infrared spectrum (FTIR, Nicolet5700) were also used to analyze the components and the formation process of the samples.
55

Electrical experiments

To provide the same test conditions for the samples, the same amount of the initial GO sheets was employed to prepare the RGO and S-RGO sheets. The tested samples would be minished
60 to a monolayered or few-layered sheet with tens of microns (no smaller than 30 μm) by finely controlling the power of ultrasonic wave or the time of ultrasonic treatment in deionized water. Then, the monolayered or few-layered sheet was floated on the surface of deionized water, subsequently transferred onto the
65 interdigitated Au electrodes with the same areas. Finally, the tested samples were dried in a vacuum oven at 60 °C for 4 h to keep fine contact with the electrodes, respectively. The electrical conductivities of the samples transferred onto the interdigitated Au electrodes were measured by a semiconductor parameter
70 analyzer (KEITHLEY 4200-SCS) with a two electrode system.

Results and Discussion

SEM and TEM characterizations

Without any polymer or surfactant, a homogeneous GO aqueous solution is readily prepared by controlling ultrasonication-assisted
75 exfoliation of graphite oxides in deionized water.[31] Subsequently, a monolayered or few-layered GO sheets can be transformed into S-RGO sheets by using Na_2S as a sulfur-doped source and a reducing agent through a hydrothermal reaction process at 200 °C in one pot. The detailed nanoscale morphologies of GO sheets
80 and S-RGO sheets are shown in Fig. 1 by a SEM. Fig. 1a shows a low-magnification SEM image of the parent GO sheets with some distinct folds and wrinkling. The high-magnification SEM image (Fig. 1b) of the parent GO sheets further offers an immediate evidence of the peeled-off GO sheets through the
85 modified Hummers' process[29] and the ultrasonic exfoliation process. These as-prepared GO sheets have some distinct folds and wrinkling on their surfaces[32] due to the oxygen-containing functional groups on the surface of GO sheet. While Fig. 1c demonstrates S-RGO sheets with more distinct folds and
90 wrinkling, very different from that of GO sheets in Fig. 1a, because the functional groups and the induced contraction of sulfur doping disrupt the original conjugation, resulting in more folds and distortions on the surface of S-RGO sheets. Furthermore, from the observation of high-magnification SEM
95 images in Fig. 1d, the surface of S-RGO sheets also shows more 'waviness' and looks like a loose stacked gauze, very different from that of GO sheets (Fig. 1b), presumably due to the induced contraction of sulfur doping in S-RGO sheets.

100
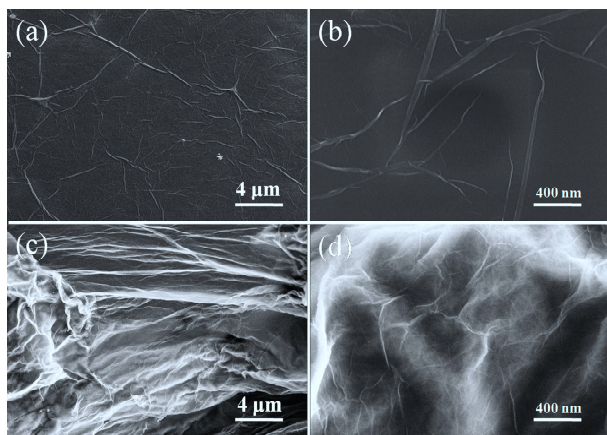
Fig. 1 SEM images of (a, b) GO sheets, and (c, d) S-RGO sheets with different magnifications.

Control experiments were carried out to demonstrate the morphological differences of GO sheets, RGO sheets and S-RGO sheets by a TEM. Fig. 2a shows that the monolayered or few-layered GO sheets have some noticeable folded traces, and Fig. 2b further reveals that these GO sheets with some distinct folds and wrinkling should be mostly a monolayer sheet. These as-prepared GO sheets would be individually well-dispersed in deionized water, because of the electrostatic repulsion of the surface charge.[33] The TEM images in Fig. 2c and d show that RGO sheets have more folds due to the aggregation and stacking between individual RGO sheets driven by the strong π-π interaction in the hydrothermal reaction process, similar to those of graphene and RGO sheets reported in the literature.[29,34] While Fig. 2e and f clearly exhibit that S-RGO sheets present a loose stacked gauze-like structure, consistent with the SEM images in Fig. 1c and d. This structure is very different from those of the above GO sheets (Fig. 2a and b) and RGO sheets (Fig. 2c and d). It is maybe due to that the introduced Na_2S plays an important role in the formation of S-RGO sheets.
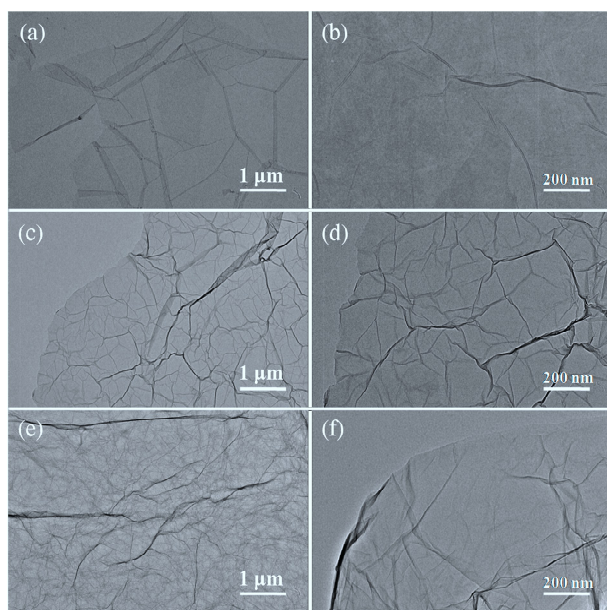
Fig. 2 TEM images of (a, b) GO sheets, (c, d) RGO sheets, and (e, f) S-RGO sheets with different magnifications.

Formation mechanism analysis

To further probe the formation mechanism of S-RGO sheets, some important features of the chemical structure of GO sheet shall be briefly described below. Oxygen-containing functional groups and other hole defects are inevitably formed in GO sheet due to the harsh oxidization of the modified Hummers' process.[29] Abundant oxygen-containing functional groups, such as phenol hydroxy and epoxide groups in the basal plane, and carboxylic groups at the lateral edges of GO sheet, offer chemically reactive sites to allow the interactions between GO sheet and various organic/inorganic materials in non-covalent, covalent and/or ionic manners.[35,36] During the hydrothermal reaction process of 200 ℃ in one pot, it is reasoned that the introduced Na_2S can act as not only a sulfur dopant, but also a reducing agent in the formation of S-RGO sheets.

To confirm the incorporation of the elemental sulfur into S-RGO sheets, the resulting samples were ultrasonically dispersed in deionized water, washed with deionized water several times to remove physical adsorption of S by filtration, and then analysed via EDX to disclose the presence of carbon (C), oxygen (O) and sulfur (S). As when the amount of Na_2S in the parent reaction solution was excessive over 27 mg, the S content could be saturated at the maximum of 2.22 at%, accompanied with C of 88.17 at% and O of 9.61 at%, as shown in Fig. 3a and b. The C atoms originate from the framework of GO sheet, the O atoms come from oxygen-containing functional groups of GO sheet, and the S atoms only originate from the elemental sulfur incorporated into the S-RGO sheet. The distributions of the C, O and S atoms in the selected region of the S-RGO sheets are clearly demonstrated by elemental mappings, particularly the uniform distribution of S atoms (Fig. 3c-e).
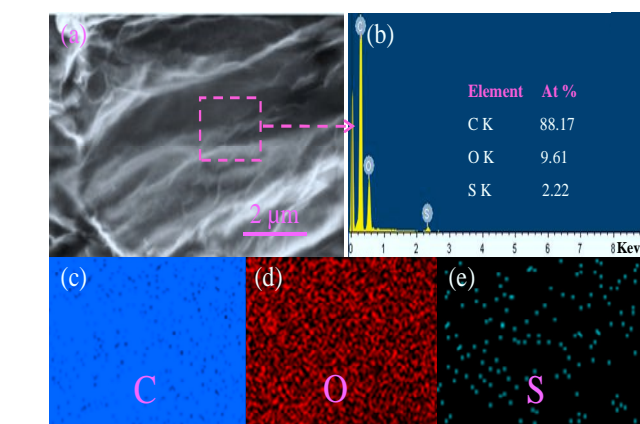
Fig. 3 (a) SEM image of S-RGO sheets with 2.22 at% sulfur doping, (b) Elemental analysis of the selected region aided by EDX, and (c-e) The C, O and S elemental mappings of the selected region.

The chemical compositions and status of the elemental sulfur in S-RGO sheets with 2.22 at% sulfur doping were further investigated using XPS in Fig. 4. The XPS survey spectra of GO sheets show the presence of only carbon and oxygen atoms (Fig. 4a). While the XPS survey spectra of S-RGO sheets reveal four peaks[5,23,26,28] corresponding to carbon (C1s), oxygen (O1s), sulfur

(S2s), and sulfur (S2p), respectively. It can be found that the O1s peak shows an apparent decrease and two weak XPS signals appear from the peaks of S2s and S2p after sulfur doping. The high-resolution S2p XPS spectrum (Fig. 4b) of the S-RGO sheets
[5] is composed of three peaks[7,18] centered at 163.1, 164.3 and 169.2 eV, corresponding to S2p$_{3/2}$ (-C-S-C-), S2p$_{1/2}$ (-C-S-C-) and oxidized sulfur groups (-C-SOx-C-), respectively. It is also noted that the S atoms dominate in the framework of S-RGO sheets via the formation of the sulfide bridges (-C-S-C). Therefore, it can be
[10] concluded that most of S atoms are directly doped into the carbon backbone of the graphene-based materials.[18]

As shown in Fig. 4c, the high-resolution C1s XPS spectrum of the original GO sheets reveals the presence of C=C/C−C (~ 284.7 eV), C−O (hydroxyl and epoxy, ~ 285.8 eV), C=O
[15] (carbonyl, ~ 286.7 eV), and O−C=O (carboxyl, ~ 288.4 eV) groups. As for the C1s XPS spectrum of the S-RGO sheets (Fig. 4d), the deconvoluted four small peaks centre at 284.7 eV (C=C/C−C), 285.5 eV (C−S/C−O),[16,25,26] 287.2 eV (C=O,) and 290.0 eV (O−C=O), respectively. After the hydrothermal
[20] treatment, the peaks of oxygen-containing functional groups were greatly reduced and the peak corresponding to the sp^2 carbon increased and became narrower. In addition, the XPS analyses reveal that the atomic ratios of C and O in GO and RGO sheets are 74.84 to 25.16 and 85.62 to 14.38, respectively. While
[25] atomic ratio of C, O and S in S-RGO sheets is 88.17, 9.61 to 2.22, consistent with the S content measured by EDX. Therefore, the C/O ratio increases from 2.97 for GO sheets and 5.95 for RGO sheets to 9.17 for S-RGO sheets, suggesting that Na$_2$S is a high-efficient reduction agent in the hydrothermal process.[37]

[30] Moreover, the high-resolution O1s XPS spectra of the pure GO sheets show three components of C=O at 531.3 eV, O−C=O at 532.2 eV, and C−O at 533.0 eV (Fig. 4e). These three peaks are also present in the XPS spectra of S-RGO sheets (Fig. 4f), but the peak of C−O decreases dramatically compared with those of
[35] C=O and O−C=O (Fig. 4e), consistent with those of C1s XPS spectra (Fig. 4c and d), indicating interactions between sulfur and oxygen.[38] Therefore, the above XPS results further suggest that GO sheets reacting with Na$_2$S can incorporate S into the S-RGO sheets to afford C-S bonded groups and remove most of oxygen-
[40] containing functional groups.
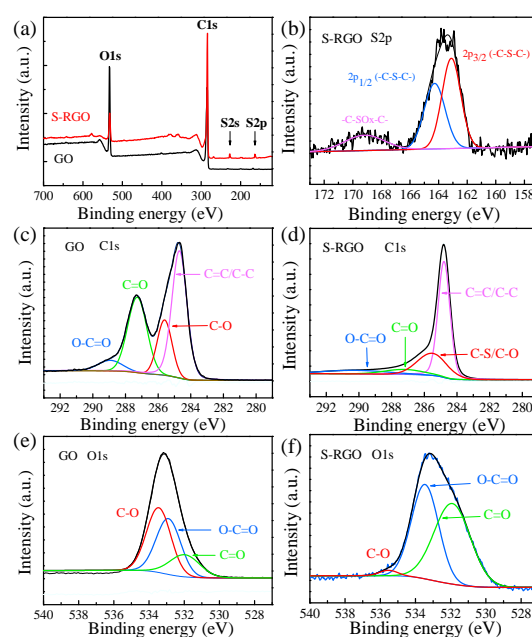
Fig. 4 (a) XPS survey spectra of GO sheets and S-RGO sheets, (b) High-resolution S2p XPS spectra of the S-RGO sheets, (c, d) High-resolution C1s XPS spectra of the GO and S-RGO sheets, and (e, f) High-resolution
[45] O1s XPS spectra of the GO and S-RGO sheets.

Further structural information of the pristine GO sheets and the resulting S-RGO sheets with 2.22 at% sulfur doping can be obtained from the XRD analysis. In the XRD patterns (Fig. 5a),
[50] GO sheets have a strong diffraction peak at 2θ =10.10° corresponding to an interlayer spacing of ~ 8.75 Å, arising from the intercalation of oxygen-containing functional groups between graphene sheets.[39] Whereas the S-RGO sheets exhibit a well-defined peak at 2θ = 24.10° corresponding to an interlayer
[55] spacing of ~ 3.68 Å, which is very close to the d-spacing of the (002) crystal plane of graphite (3.35 Å),[40] indicating the partial restoration of sp^2 carbon. Thus, the XRD results also suggest the efficient structural restoration of the graphitic framework during the hydrothermal reaction process.

[60] Raman and FTIR analyses are also performed on the pristine GO sheets and the resulting S-RGO sheets with 2.22 at% sulfur doping. Both a D peak (~ 1350 cm^{-1}) and a G peak (~ 1595 cm^{-1}) are present in the Raman spectra of GO sheets and S-RGO sheets (Fig. 5b). The intensity ratio of the D band to the G band (I$_D$/I$_G$)
[65] increases from 0.86 for GO sheets to 1.10 for S-RGO sheets due to a part restoration of the graphitic framework and the additional defect stabilization by sulfur doping.[21,23] The FTIR spectra of the pristine GO sheets (Fig. 5c) have proved the presence of different functional groups, such as O–H stretching vibration around 3430
[70] cm^{-1}, C–H stretching vibration around 2981 cm^{-1} and 1405 cm^{-1}, C=O stretching mode at 1723 cm^{-1}, C=C stretching vibration around 1622 cm^{-1}, C–OH stretching vibration at 1250 cm^{-1}, and C–O stretching mode at 1050 cm^{-1}. In addition, the relative intensities of O–H, C=O, C–H, C–OH, and C–O are greatly
[75] reduced from the pristine GO sheets to the resulting S-RGO sheets, also implying that the degree of sp^2 domains in the S-RGO sheets appears an apparent increase.[38]
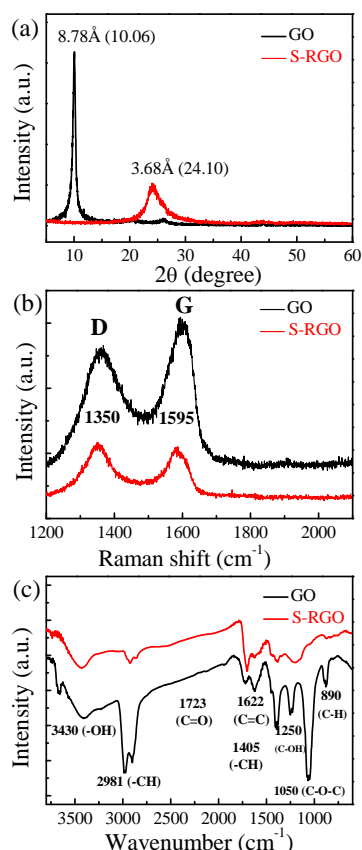
Fig. 5 (a) XRD patterns, (b) Raman spectra, and (c) FTIR spectra of GO sheets and S-RGO sheets with 2.22 at% sulfur doping.

The XPS results coupled with EDX, XRD, Raman and FTIR analyses strongly confirmed that the S atoms have been successfully introduced into the graphene framework via covalent bonds, and sulfur doping of graphene can be achieved using our approach. The formation of C-S bond is attributed to the reaction between oxygen containing groups of GO sheet and Na_2S. The introduced Na_2S acts as not only a sulfur dopant, but also a reducing agent in the formation of S-RGO sheets through the hydrothermal reaction process at moderate temperature of 200 °C in one pot.

Electrical property of S-RGO sheets

The resulting S-RGO sheets with 2.22 at% sulfur doping transferred onto the interdigitated Au electrodes at about 30 μm intervals (Fig. 6a and b) show high conductivity, which can be confirmed by the current-voltage (*I-V*) curve. For comparison, the electrical conductivities of GO sheets, RGO sheets and a single-layer CVD-grown graphene sheets were also measured. The *I-V* curve of GO sheets exhibits a very low current of about 2.5 μA at a high applied bias of 5.0 V (Fig. 6c), suggesting that GO sheets are almost electrically insulating. The current value of RGO sheets is about 1.2 mA at an applied bias of 2.0 V (Fig. 6d). While the electrical conductivity of the S-RGO sheets can enhance with the increasing atomic percentage of S (0-2.22 at%), as when it reaches to a maximum of 2.22 at%, about 50.0 mA current passes through the resulting S-RGO sheets at an applied

bias of 2.0 V (Fig. 6e). This current value is much higher than that of RGO sheets (~ 1.2 mA) (Figure 6d) and very close to that of the CVD-made single-layer graphene (~ 68.0 mA) at the same applied bias (Fig. 6f). In fact, the ohmic contact in Fig. 6 for all the samples also confirms the fine electrical connection. The difference between the conductivity of the GO sheet and the graphene sheet is mainly ascribed to the breakthrough of conductive sp^2 network in the graphene sheet by replacement of some sp^3 carbon sites.[41,42]

Based on the EDX, XPS, XRD, Raman and FTIR analyses mentioned above, the introduced Na_2S can act as not only a sulfur dopant, but also a high-efficient reducing agent in the formation of S-RGO sheets, thus the elemental sulfur is incorporated into S-RGO sheets and a part of the graphitic framework is restored in the hydrothermal reaction process. The synergistic effects of a sulfur dopant and a reducing agent improve dramatically the electrical conductivities of the resulting S-RGO sheets, compared with other previous reports.[41,43]
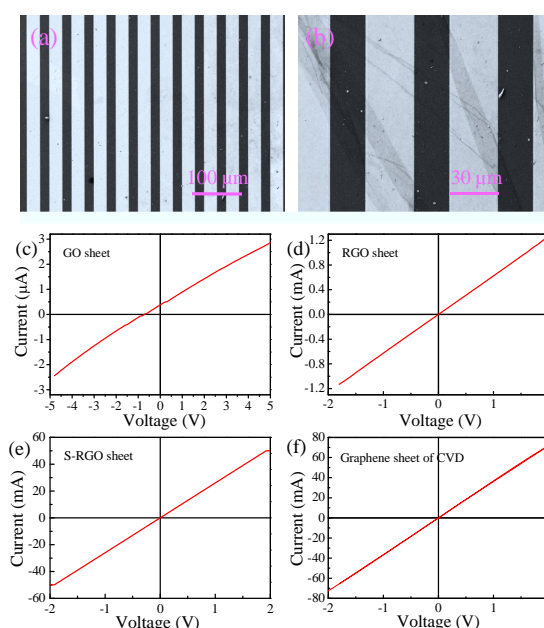
Fig. 6 SEM images of (a) the interdigitated Au electrodes with about 30 μm intervals on rigid ceramic substrate, and (b) S-RGO sheets with 2.22 at% sulfur doping transferred onto the interdigitated Au electrodes. *I-V* curves of (c) GO sheets, (d) RGO sheets, (e) S-RGO sheets with 2.22 at% sulfur doping, and (f) a single-layer graphene of CVD.

Conclusion

In this study, we demonstrated the facile synthesis of S-RGO sheets with excellent electrical properties by only using GO sheets and Na_2S as precursors through a mild hydrothermal reaction process at 200 °C in one pot without any polymer or surfactant. The S-RGO sheets can be normally fabricated on a large scale. As when the atomic percentage of S reaches to a maximum of 2.22 at%, about 50.0 mA current passes through the resulting S-RGO sheet at an applied bias of 2.0 V. This current value is much higher than that of the RGO sheet (~ 1.2 mA) and very close to that of the single-layer graphene sheet made by CVD (~ 68.0 mA) under the same test conditions. During the

hydrothermal reaction process, the introduced Na_2S can act as not only a sulfur dopant, but also a reducing agent in the formation of S-RGO sheets. The synergistic effects of a sulfur dopant and a reducing agent improve dramatically the electrical conductivities of the resulting S-RGO sheets. These highly conductive S-RGO sheets offer many promising technological applications such as efficient metal-free electrocatalysts in oxygen reduction reaction for fuel cells and supercapacitor electrode materials for high-performance Li-ion batteries. Systematic investigations are underway to further clarify the nature of the enhancement mechanism of the electrical conductivities of the resulting S-RGO sheets.

Acknowledgements

Notes and references

aSchool of Chemistry and Chemical Engineering, Pingdingshan University, Pingdingshan 467000, P. R. China.
bState Key Laboratory of Bioelectronics, School of Biological Science and Medical Engineering, Southeast University, Nanjing 210096, P. R. China.

* Corresponding Author: *E-mail*: xcxseu@seu.edu.cn

1 Y. D. Kim, H. Kim, Y. Cho, J. H. Ryoo, C.-H. Park, P. Kim, Y. S. Kim, S. Lee, Y. Li, S.-N. Park, Y. S. Yoo, D. Yoon, V. E. Dorgan, E. Pop, T. F. Heinz, J. Hone, S.-H. Chun, H. Cheong, S. W. Lee, M.-H. Bae and Y. D. Park, Nat. Nanotechnol., 2015, **10**, 676-681.

2 Q. Zhou, J. Zheng, S. Onishi, M. F. Crommie and A. K. Zettl, P. Natl. Acad. Sci. USA , 2015, **112** , 8942-8946.

3 M. Singh, M. Holzinger, M. Tabrizian, S. Winters, N. C. Berner, S. Cosnier and G. S. Duesberg, J. Am. Chem. Soc., 2015, **137**, 2800-2803.

4 Z. Wu, Z. Liu, K. Parvez, X. Feng and K. Müllen, *Adv. Mater.*, 2015, **27**, 3669-3675.

5 X. Chen, X. Chen, X. Xu, Z.Yang, Z. Liu, L. Zhang, X. Xu, Y. Chen and S. Huang, Nanoscale, 2014, **6**, 13740-13747.

6 X. Liu and M. Antonietti, Adv. Mater., 2013, **25**, 6284-6290.

7 Z. Yang, Z. Yao, G. Li, G. Fang, H. Nie, Z. Liu, X. Zhou, X. Chen and S. Huang, ACS Nano, 2012, **6**, 205-211.

8 Y. Zhang, T.-T. Tang, C. Girit, Z. Hao, M. C. Martin, A. Zettl, M. F. Crommie, Y. R. Shen and F. Wang, Nature, 2009, **459**, 820-823

9 X. Li, S. P. Lau, L. Tang, R. Ji and P. Yang, Nanoscale, 2014, **6**, 5323-5328.

10 X. Kong, C. Chen and Q. Chen, Chem. Soc. Rev., 2014, **43**, 2841-2857.

11 X. Wang, G. Sun, P. Routh, D.-H. Kim, W. Huang and P. Chen, Chem. Soc. Rev., 2014, **43**, 7067-7098.

12 Y. Chen, J. Li, T. Mei, X. Hu, D. Liu, J. Wang, M. Hao, J. Li, J. Wang and X. Wang, *J. Mater. Chem. A*, 2014, **2**, 20714-20722.

13 D. R. Dreyer, S. Park, C. W. Bielawski and R. S. Ruoff, *Chem. Soc. Rev.*, 2010, **39**, 228-240.

14 Z. Xu and C. Gao, *Nat. Commun.*, 2011, **2**, 571.

15 H. Y. Park, T. J. Shin, H. I. Joh, J. H. Jang, D. Ahn and S. J. Yoo, Electrochem Commun., 2014, **41**, 35-38.

16 H. L. Poh, P. Šimek, Z. Sofer and M. Pumera, *ACS Nano.*, 2013, **7**, 5262-5272.

17 S. Yang, L. Zhi, K. Tang, X. Feng, J. Maier and K. Müllen, *Adv. Funct. Mater.*, 2012, **22**, 3634-3640.

18 Y. Zhang, M. Chu, L. Yang, W. Deng, Y. Tan, M. Ma and Q. Xie, *Chem. Commun.*, 2014, **50**, 6382-6385.

19 J. Wang, R. Ma, Z. Zhou, G. Liu and Q. Liu, *Sci. Rep.*, 2015, **5**, 9304.

20 M. A. Hoque, F. M. Hassan, D. Higgins, J.-Y. Choi, M. Pritzker, S. Knights, S. Ye and Z. Chen, *Adv. Mater.*, 2015, **27**, 1229-1234.

21 Z. Ma, S. Dou, A. Shen, L. Tao, L. Dai and S. Wang, *Angew. Chem. Int. Ed.*, 2015, **54**, 1888 -1892.

22 D. Higgins, M. A. Hoque, M. H. Seo, R. Wang, F. Hassan, J.-Y. Choi, M. Pritzker, A.Yu, J. Zhang and Z. Chen, *Adv. Funct. Mater.*, 2014, **24**, 4325-4336.

23 X. Ma, G. Ning, Y. Sun, Y. Pu, J. Gao, *Carbon*, 2014, **79**, 310-320.

24 Y. Yan, Y. X. Yin, S. Xin, Y. G. Guoand L. J. Wan, *Chem. Commun.*, 2012, **48**, 10663-10665.

25 W. Ai, Z. Luo, J. Jiang, J. Zhu, Z. Du, Z. Fan, L. Xie, H. Zhang, W. Huang and T. Yu, *Adv. Mater.*, 2014, **26**, 6186-6192.

26 G. Chen, Y. Liu, Y. Liu, Y. Tian and X. Zhang, J. Electroanal. Chem., 2015, **738**, 100-107.

27 C. Liang, Y. Wang and T. Li, *Carbon*, 2015, **82**, 506-512

28 Z. Wang, P. Li, Y. Chen, J. He, W. Zhang, O. G. Schmidt and Y. Li, *Nanoscale*, 2014, **6**, 7281-7287.

29 S. Park and R. S. Ruoff, *Nat. Nanotechnol.*, 2009, **4**, 217-224.

30 X. Li, W. Cai, J. An, S. Kim, J. Nah, D. Yang, R. Piner, A. Velamakanni, I. Jung, E. Tutuc, S. K. Banerjee, L. Colombo and R. S. Ruoff, *Science*, 2009, **324**, 1312-1314.

31 Z. Tian, C. Xu, J. Li, G. Zhu, Z. Shi and Y. Lin, *J. Nanosci. Nanotechnol.*, 2015, **15**, 2015-2019.

32 Z. Tian, C. Xu, J. Li, G. Zhu, Z. Shi and Y. Lin, *ACS Appl. Mater. Interfaces*, 2013, **5**, 1489-1493.

33 D. Li, M. B. Müller, S. Gilje, R. B. Kaner and G. G. Wallace, *Nat. Nanotechnol.*, 2008, **3**, 101-105.

34 Y. X. Xu, K. X. Sheng, C. Li, G. Q. Shi, *ACS Nano*, 2010, **4**, 4324-4330.

35 D. A. Dikin, S. Stankovich, E. J. Zimney, R. D. Piner, G. H. Dommett, G. Evmenenko, S. T. Nguyen and R. S. Ruoff, *Nature*, 2007, **448**, 457-460.

36 K. Erickson, R. Erni, Z. Lee, N. Alem, W. Gannett and A. Zettl, *Adv. Mater.*, 2010, **22**, 4467-4472

37 S. Pei, J. Zhao, J. Du, W. Ren and H.-M. Cheng, *Carbon*, 2010, **48**, 4466-4474.

38 Y. S. Yun, V.-D. Le, H. Kim, S.-J. Chang, S. J. Baek, S. Park, B. H. Kim, Y.-H. Kim, K. Kang, H.-J. Jin, *J. Power Sources*, 2014, **262**, 79-85.

39 S. Song, Y. Xue, L. Feng, H. Elbatal, P. Wang, C. N. Moorefield, G. R. Newkome, L. Dai, *Angew. Chem. Int. Ed.*, 2014, **53**, 1415-1419.

40 Z. Tian, C. Xu, J. Li, G. Zhu, P. Li, J. Dai and Z. Shi, *Sci. Adv. Mater.*, 2015, **7**, 1415-1423

41 M. R. Karim, H. Shinoda, M. Nakai, K. Hatakeyama, H. Kamihata, T. Matsui, T. Taniguchi, M. Koinuma, K. Kuroiwa, M. Kurmoo, Y. Matsumoto and S. Hayami, *Adv. Funct. Mater.*, 2013, **23**, 323-332.

42 H. Liu, L. Zhang, Y. Guo, C. Cheng, L. Yang, L. Jiang, G. Yu, W. Hu, Y. Liu and D. Zhu, *J. Mater. Chem. C*, 2013, **1**, 3104-3109.

43 Z. Tian, C. Xu, J. Li, G. Zhu, J. Wu, Z. Shi and Y. Wang, *New J. Chem.*, 2015, **39**, 6907-6913.